17th World Conference on Earthquake Engineering, 17WCEE
Sendai, Japan - September 13th to 18th 2020

COMPARISON OF 3D STRESS-STRAIN CONCRETE MODELS

M.F. Chacón[1], J.C. de la Llera[2], M.A. Hube[3] and D. Celentano[4]

[1] *Postdoctoral researcher, Department of Structural and Geotechnical Engineering and Research Center for Integrated Disaster Risk Management (CIGIDEN), CONICYT/FONDAP/15110017, Pontificia Universidad Católica de Chile,* mfchacon@uc.cl
[2] *Professor, Department of Structural and Geotechnical Engineering* and *CIGIDEN, Pontificia Universidad Católica de Chile,* jcllera@ing.puc.cl
[3] *Associated professor, Department of Structural and Geotechnical Engineering and CIGIDEN, Pontificia Universidad Católica de Chile,* mhube@ing.puc.cl
[4] *Professor, Department of Mechanical and Metallurgical Engineering, Pontificia Universidad Católica de Chile,* dcelentano@ing.puc.cl

Abstract

The inelastic response of reinforced concrete buildings is strongly sensitive to the material stress-strain constitutive model adopted for concrete. This paper is a first step on an ongoing work to do a complete benchmark analysis of available concrete models. Consequently, this article quantifies the differences in the response of three well-known 3D stress-strain continuum concrete models: **(i)** the Hyperbolic Drucker-Prager (DPH) plastic model; **(ii)** the UNIlateral (UNI) damage model; and **(iii)** the Faría-Oliver-Cervera (FOC) plastic-damage model. Consistent algorithms in terms of the updated stresses and the tangent stiffness tensor for all these models were implemented in the ANSYS software using user-material FORTRAN routines adapted to solid-type finite elements. Models results were validated using a set of experimental benchmark tests subjected to uniaxial and biaxial stress states under monotonic and cyclic loading. Moreover, the unilateral (crack opening-and-closure) effect was compared among these models. A set of ten response parameters were compared relative to the experimental tests, e.g., the peak stress, the unloading stiffness at each loading cycle, and the total dissipated energy. Results show that the dissipated energy and the unloading stiffness in the last loading cycle, for all tests, leads to the largest errors.

Keywords: 3D continuum concrete models, numerical implementation, benchmark tests, plastic-damage concrete models.

1. Introduction

Thanks to the latter advances in supercomputers, Reinforced Concrete (RC) buildings structural models can be used to predict the seismic response with a considerable reduction in CPU time producing a large amount of valuable data. Such nonlinear analyses require to evaluate the inelastic dynamic response and identify the potential damage zones [1][2]. Because concrete is a brittle material that exhibits a strongly nonlinear response associated with the propagation of cracking, its numerical modeling is challenging and requires robust algorithms to achieve convergence. The incorporation of nonlinear stress-strain constitutive concrete models is the key ingredient to predict with accuracy and speed the inelastic behavior of RC structures. Moreover, the use of these micro-models in Finite Element (FE), and Three-Dimensional (3D) or plane-stress concrete formulations, allow simulating detailed stress and strain field distributions under complex structural geometries and multi-axial loading conditions [3][4][5], as it is the case of large structures [3][6].

In the past thirty years, many 3D and plane-stress concrete constitutive models have been elaborated to describe the mechanical behavior of concrete under multi-axial stress loadings. Five main groups of concrete models can be distinguished: **(i)** plastic models, which considers the flow plasticity theory to describe the plastic strains and hardening behavior, where a non-associated flow rule and a single- or multi-surface yield criterion is considered to distinguish between compression and tension behavior (e.g., Mohr-Coulomb, [7][8][9]; **(ii)** damage models, which are based on Continuum Damage Mechanics (CDM) [10], which assume the thermodynamic of irreversible damage process to simulate the stiffness degradation and strain-softening

behavior due to micro-crack propagation. It can include scalar variables to characterize the isotropic damage process [11][12][13] or a tensorial variables to describe the anisotropic damage effects [14]; **(iii)** plastic-damage models, which combine the plasticity and CDM theories [12][13][15][16]; **(iv)** fracture models, based on the nonlinear fracture mechanics theory [17][18][19]; and **(v)** mixed models, that combine plastic-damage, smeared crack, or fracture-plastic models [20][21].

For strain-driven models, the numerical implementation of concrete models consists in two main steps: (i) an updated stress tensor algorithm given a strain increment; and (ii) a consistent stiffness tensor according to the updated stress. Implicit integration schemes with Return-Mapping Algorithms (RMA) are generally used for plastic and plastic-damage models [22][23], whereas explicit integration schemes are considered for damage and smeared crack models [12]. Most of these algorithms are implemented in FE software using local models, where the stress at each integration point is dependent only on their respective strain. Convergence problems arise in local models of materials with softening behavior due to strain-localization, leading to spurious mesh sensitivity and unreliable results [24]. Local models can be improved with different methods that include an intrinsic length scale in the continuum equations, such as higher-order gradients [25], non-local media [24], or rate-dependent terms [26]. Inner the possibilities, the rate-dependent approach is the most adequate and easier to implement for plastic and damage concrete models. The incorporation of a numerical viscosity in the stress-strain constitutive equations improves the convergence greatly, but at the expense of a gradual overstress condition depending on the strain-rate increment.

Each material model formulation uses different assumptions and constitutive equations, which is associated with a level of knowledge or approximation to the experimental behavior of the material. Moreover, each model uses different notation and input parameters, which gives different responses and are difficult to compare among them. Both classes of uncertainty are classified as epistemic and are quantified in this paper. The epistemic uncertainty can be quantified by at least three methodologies: **(i)** stochastic models, where the variables distribute according to a probability density function, for which several amounts of cases are generated with Monte Carlo simulations [27]; **(ii)** sensitivity simulations, where some parameters lie on a range of possible discrete values; and **(iii)** empirical data and reduction of uncertainty through model calibrations using real data. There is scarce research on the uncertainty of inelastic concrete model simulations for pure concrete structures where their responses are compared using different numerical concrete models. Some examples are found, such as experimental test specimens [28], double-edge-notched specimens [29], impact loads tests [30], or simple numerical concrete tests [31]. A good quantification of the variability in the response of a set of numerical concrete models can give a better understanding of the uncertainty of the response of RC structures.

The objective of this paper is to quantify the errors associated with the response of three different 3D continuum concrete models. Section 2 presents a brief description of the theory behind the concrete models considered. Numerical examples using basic experimental benchmarks tests subject to monotonic and cyclic loading conditions under uniaxial and biaxial stresses are presented in Section 3. Finally, Section 4 quantifies the error of concrete models with a set of ten response parameters of the numerical tests considered.

2. Inelastic concrete models

2.1 Overview of theoretical formulations

This section presents a rough overview of the three inelastic concrete models considered in this article, showing some of the equations and properties. Modifications were incorporated into original models [32][33] to improve their convergence.

Drucker-Prager Hyperbolic (DPH) model

This plastic model, known also as the "Extended Drucker-Prager" model, was defined by Drucker & Prager [7] and modified by [34][35]. The model considers a cone shape yield surface to simulate the pressure-dependent behavior and the asymmetric tensile/compressive strength of concrete (see Fig. 1a). It also includes

a smoothed hyperbolic flow potential surface that controls the inelastic volumetric strain rate (dilatancy). The advantage of this surface is to avoid the singularity at the cone's apex present in the classical Drucker-Prager model, giving a unique flow tensor through the entire surface, which improves the convergence at the tensile regime (see Fig. 1b).

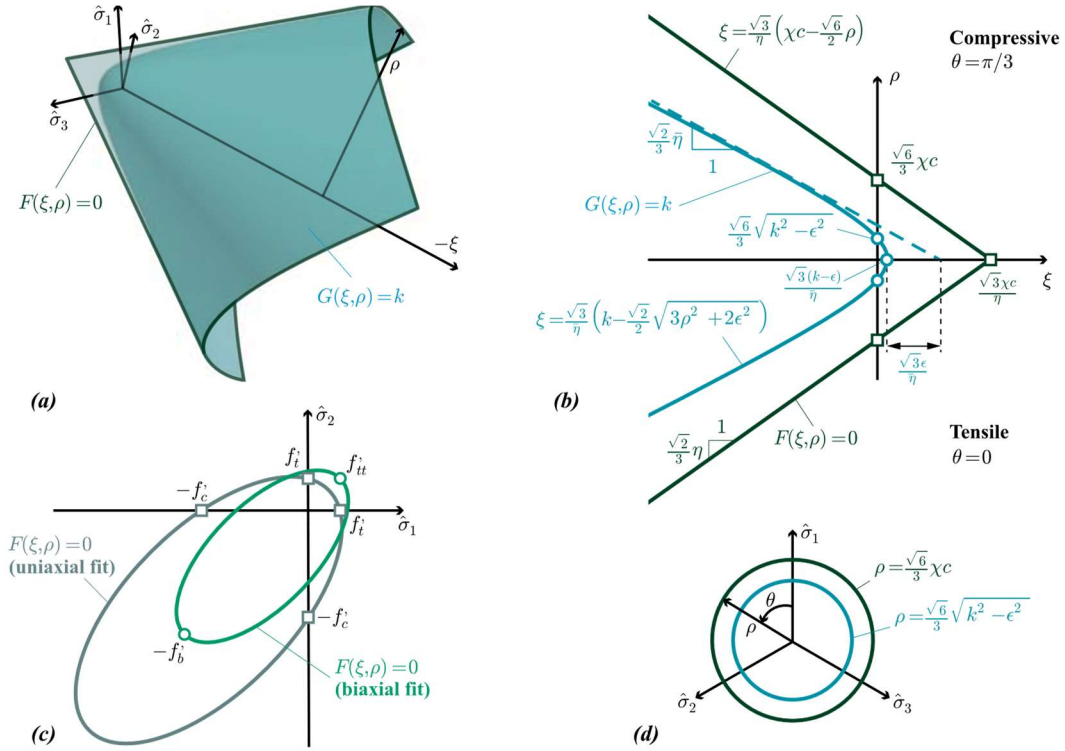

Fig. 1 – Yield criterion of the DPH model: (a) 3D view in principal stress; (b) tensile/compressive meridians in Rendulic plane; (c) biaxial-stress plane; and (d) deviatoric π-plane. The following parameters were used: f_t'=6 MPa, f_c'=20 MPa, $f_b' = 1.16 f_c'$.

Unilateral (UNI) model

This damage model was first established by Ladeveze [36], Mazars & Pijaudier-Cabot [37], and latter reformulated by Faría & Oliver [12]. The model neglects plastic strains, and assumes that the effective stress tensor $\bar{\boldsymbol{\sigma}}$ is elastic, which can be split into positive $\bar{\boldsymbol{\sigma}}^+$ and negative $\bar{\boldsymbol{\sigma}}^-$ parts, to account separately for the cracking (tension) and shear (compression) damage mechanisms for degradation of concrete using the spectral decomposition [14]. Furthermore, for the damage component, the model considers the definition of a damaged Helmholtz free energy potential in order to satisfy the thermodynamically irreversible damage process.

Faría -Oliver-Cervera (FOC) model

This plastic-damage model was proposed by Faría & Oliver [12]. The model considers an identical effective stress decomposition and the damage component than the UNI model and uses a simplified representation of the evolution of the plastic strain in an explicit scheme.

Table 1 shows the constitutive equations considered to calculate the plastic, damage, and nominal component of the stress tensor for each concrete model, respectively. Additionally, the UNI and FOC models can be extended to include a strain-rate dependency through the Duvaut-Lions [38] visco-plastic model. This approach is forced because improves considerably the convergence of the models in strain-softening regimes. More details of these additional equations are explained elsewhere [32]. The unique parameter that controls the strain-rate increment is the numerical viscosity μ_v and is equivalent to the relaxation time.

Table 1 – Constitutive equations of the plastic, damage, and nominal component of the stress tensor of the inelastic concrete models.

	Plastic component			
	Stress	**Yield criterion**	**Flow rule**	**Evolution hardening law**
DPH	$\boldsymbol{\sigma} = \boldsymbol{\mathcal{D}}^e : (\boldsymbol{\varepsilon} - \boldsymbol{\varepsilon}^p)$	$F(\boldsymbol{\sigma}, \alpha) = \eta p + q - \chi c(\alpha)$	$\dot{\boldsymbol{\varepsilon}}^p = \dot{\gamma}\boldsymbol{N}, \quad \boldsymbol{N} = \frac{3}{2r}\boldsymbol{s} + \frac{\bar{\eta}}{3}\boldsymbol{I}$	$\dot{\alpha} = \dot{\gamma}\chi$
UNI	-	-	-	-
FOC	$\bar{\boldsymbol{\sigma}} = \boldsymbol{\mathcal{D}}^e : (\boldsymbol{\varepsilon} - \boldsymbol{\varepsilon}^p)$	-	$\dot{\boldsymbol{\varepsilon}}^p = \dot{\gamma}\boldsymbol{N}, \quad \boldsymbol{N} = \bar{\boldsymbol{\sigma}}, \quad \dot{\gamma} = E_o \lambda \frac{\langle \boldsymbol{\varepsilon}^e : \dot{\boldsymbol{\varepsilon}} \rangle^+}{(\bar{\boldsymbol{\sigma}} : \bar{\boldsymbol{\sigma}})}$	-

	Damage component	**Nominal stress**
DPH	-	-
UNI	$\omega^{\pm} = \omega^{\pm}(r^{\pm}), \quad r^{\pm} = \max\left(r_o^{\pm}, \max_{[0,t]}(Y^{\pm})\right), \quad Y^{\pm} = \sqrt{E_o(\bar{\boldsymbol{\sigma}}^+ : \boldsymbol{\mathcal{C}}^e : \bar{\boldsymbol{\sigma}})}, \quad Y^- = \eta\bar{p} + \bar{q} + \delta\langle\hat{\bar{\sigma}}_{\max}\rangle^-$	$\boldsymbol{\sigma} = (1-\omega^+)\bar{\boldsymbol{\sigma}}^+ + (1-\omega^-)\bar{\boldsymbol{\sigma}}^-, \quad \bar{\boldsymbol{\sigma}}^{\pm} = \boldsymbol{\mathcal{P}}^{\pm} : \bar{\boldsymbol{\sigma}}, \quad \boldsymbol{\mathcal{P}}^{\pm} = \sum_{i=1}^{N} H_0^{\pm}(\hat{\bar{\sigma}}_i)\,(\boldsymbol{E}_{\bar{\sigma}}^{ii} \otimes \boldsymbol{E}_{\bar{\sigma}}^{ii})$
FOC	idem to UNI	idem to UNI

In all cases: $\boldsymbol{\varepsilon} = \boldsymbol{\varepsilon}^e + \boldsymbol{\varepsilon}^p$ total strain tensor, $\boldsymbol{\sigma}$ nominal stress tensor, $\bar{\boldsymbol{\sigma}}$ effective stress tensor, $q = \sqrt{\frac{3}{2}\boldsymbol{s}:\boldsymbol{s}}$, $p = \frac{1}{3}(\boldsymbol{I}:\boldsymbol{\sigma})$, $r = \sqrt{q^2 + \epsilon^2}$, and N is the dimension of problem (for 3D case, N=3). The spectral decomposition of a symmetric second-order tensor $\boldsymbol{A}$ is defined as $\boldsymbol{A} = \underline{\boldsymbol{V}}\underline{\hat{\boldsymbol{A}}}\underline{\boldsymbol{V}}^{\boldsymbol{T}} = \sum_{i=1}^{N} \hat{a}_i \boldsymbol{E}_a^{ii}$, where $\hat{a}_i$ is the i-th eigenvalue and $\boldsymbol{E}_a^{ii} = \underline{\boldsymbol{v}}^i \otimes \underline{\boldsymbol{v}}^i$ the i-th eigen-projector tensor, with $\underline{\boldsymbol{v}}^i$ is the i-th column of the eigenvector matrix $\underline{\boldsymbol{V}}$. For the DPH model: ϵ is the eccentricity parameter; UNI model: $r_o^+ = \sigma_o^+$, $r_o^- = (1-\alpha)\sigma_o^-$, where $\sigma_o^{\pm}$ are the stress onset tensile/compressive nonlinear behavior, respectively.

Finally, Table 2 shows the main capabilities for the described concrete models. Classification of models (plastic, damage, plastic-damage), strain-softening behavior, stress state effects (biaxial or triaxial), dilatancy, unilateral effect, and strain-rate effect are mentioned. The table also presents the inelastic input parameters.

Table 2– Properties of concrete models and their input parameters.

		Properties						**Inelastic inputs**	
Model	**Class**	**Softening**	**Biaxial**	**Triaxial**	**Dila-tancy**	**Uni-lateral**	**Strain-rate**	**Scalar**	**Uniaxial laws**
DPH	P		✓	✓	✓			$\eta, \bar{\eta}, \xi, \epsilon$	$c(\alpha)$
UNI	D	✓	✓	✓		✓	✓	f_c', f_b', K_c, μ_v	$\omega^{\pm}(r^{\pm})$
FOC	PD	✓	✓	✓		✓	✓	$f_c', f_b', K_c, B^{\pm}, \mu_v$	$\omega^{\pm}(r^{\pm})$

P: plastic, D: damage, and PD: plastic-damage.

2.2 Numerical implementation and convergence issues

This section describes the main steps used for the numerical implementation and gives some recommendations to get convergence of the concrete models. To incorporate the above concrete models in FE software requires a robust numerical implementation of the constitutive equations. In all cases, a strain-driven scheme is considered, with an algorithm to evaluate the updated stress tensor $\boldsymbol{\sigma}_{n+1}$ and internal state variables at each integration point. In the DPH model, the plastic component is evaluated with a backward Euler (implicit) scheme, where an RMA scheme composed of a trial elastic-predictor step and a plastic-corrector step is considered [22]. Conversely, in the FOC model, the plastic component is evaluated in an explicit scheme. For the DPH model, the RMA solve the consistency operator γ through an iterative Newton's method. For this method, the election of an adequate initial value, non-zero derivatives, and a unique scalar variable to be solved rather than a system of equations is critical for the convergence. Thus, enforcement of the consistency condition is used to reduce the solution to a simple scalar nonlinear equation. Conversely, the damage component of all models is evaluated with an explicit scheme.

For the numerical integration of models, the consistent tangent stiffness tensor $\frac{\partial \boldsymbol{\sigma}_{n+1}}{\partial \boldsymbol{\varepsilon}_{n+1}}$ need to be computed, which requires the derivatives of equations involved to evaluate the updated stress tensor $\boldsymbol{\sigma}_{n+1}$. For the models developed, this consistent tensor can be obtained in explicit expressions, which are derived in detail elsewhere [32]. The sensitivity to this operator in the convergence of models at the FE level is well known. Thus, to improve convergence we recommend the use of continuous and smooth derivatives (C^1-class) to elaborate this operator, being especially important in strain-softening regimes. Analogously, we recommend the use of smooth C^2-class functions for the flow potential of the DPH model; and the use of C^1-class functions for the uniaxial laws ($\sigma^{\pm}(\varepsilon^{\pm})$ or $\omega^{\pm}(r^{\pm})$) for all models. In addition, the use of any asymmetric Newton-Raphson solver is mandatory if the stiffness matrix is non-symmetric. The incorporation of all these improvements is explained in detail in [33]. Finally, it is recommended to use a ratio of numerical viscosity to load step increments $\mu_v/\Delta t$ between 0.001 and 1.0 to get adequate convergence without compromising accuracy in the response.

3. Numerical tests

In this section, a set of numerical examples is used to validate the capabilities of the constitutive concrete models described in Section 2. Taking the numerical algorithms detailed in [32][33], the three concrete models were implemented in the software ANSYS [34] through user-material FORTRAN77 routines (USERMAT.f). These material routines work at the Gauss integration point level of each finite element.

Four experimental benchmark tests were simulated with a single-element according to the following loading conditions: **(i)** cyclic uniaxial tensile; **(ii)** cyclic uniaxial compression; **(iii)** monotonic biaxial; and **(iv)** cyclic uniaxial tension-compression. All examples were modeled using 8-node solid brick element (SOLID185) with three degrees of freedom at each node using 2×2×2 Gauss integration scheme. In all cases, except for the biaxial test, a pure uniaxial stress state for the boundary constraints is imposed. For the DPH model, an exponential relation is considered for the cohesion law $c(\alpha)$ given by $c(\alpha) = c_u + (c_y - c_u)\exp(-\alpha/\alpha_o)$, where $c_u = R_1 c_y$, $\alpha_o = R_2 c_u/E_0$, c_y is the cohesion yield, $R_1, R_2 \geq 1$ are experimentally fitted parameters, and E_0 is the concrete Young's modulus. For the UNI and FOC models, the exponential relation of Oliver *et al.* [39] and Mazars [40] for the tensile/compressive uniaxial stress laws $\sigma^{\pm}(\varepsilon^{+})$ are assumed, respectively, and given by

$$\sigma^{+}(\varepsilon^{+}) = \begin{cases} \frac{f_t'}{\varepsilon_0^{+}}\varepsilon^{+} & \text{for } \varepsilon^{+} < \varepsilon_0^{+} \\ f_t'\left[1 - A^{+} + A^{+}\exp\left(B^{+}\left(1 - \frac{\varepsilon^{+}}{\varepsilon_0^{+}}\right)\right)\right] & \text{for } \varepsilon^{+} \geq \varepsilon_0^{+} \end{cases} \quad \text{and} \quad (1)$$

$$\sigma^{-}(\varepsilon^{-}) = \begin{cases} \frac{f_o^{-}}{\varepsilon_0^{-}}\varepsilon^{-} & \text{for } \varepsilon^{-} < \varepsilon_0^{-} \\ f_o^{-}\left[1 - A^{-} + \frac{A^{-}}{\varepsilon_0^{-}}\varepsilon^{-}\exp\left(B^{-}\left(1 - \frac{\varepsilon^{-}}{\varepsilon_0^{-}}\right)\right)\right] & \text{for } \varepsilon^{-} \geq \varepsilon_0^{-} \end{cases}, \quad (2)$$

where $\varepsilon_0^{+} = f_t'/E_0$ and $\varepsilon_0^{-} = f_o^{-}/E_0$, with f_o^{-} and B^{-} parameters calculated in an iterative process in order to dissipate a specific value of fracture energy G_f^{-} under the stress-strain $\sigma^{-}(\varepsilon^{-})$ curve (see [33]). For the UNI and FOC models, an explicit conversion from the $\sigma^{\pm}(\varepsilon^{\pm})$ uniaxial laws to $\omega^{\pm}(r^{\pm})$ is presented elsewhere [33]. Table 3 lists the material parameters adopted for each benchmark test. Additional parameters are listed in the figure captions of each example.

Table 3– List of parameters used in the concrete models.

Author	Test	B mm	H mm	l_c mm	E_o GPa	ν -	f_t' MPa	f_c' MPa	$G_f^{+(1)}$ N/mm	$G_f^{-(1)}$ N/mm	K_c -
Gopalaratnam & Shah [43]	1D+	82.6	82.6	82.6	31.0	0.18	3.48	27.6	0.04	11.38	1.0
Karsan & Jirsa [44]	1D-	82.6	82.6	82.6	31.7	0.2	3.48	27.6	0.04	11.38	1.0
Kupfer *et al.* [45]	2D	200	50	200	31.0	0.15	3.5	32.06	2.0	80.0	1.0
Mazars *et al.* [46]	U	80	80	80	16.4	0.2	1.4	18.1	0.011	7.0	1.0

(1) Values used in the UNI model as reference. For all cases: $f_b' = 1.16 f_c'$, $\epsilon = 0.001$, $z_c^+ = 0$, $z_c^- = 1$, $\mu_v = 0$, unless otherwise indicated. 1D+: cyclic uniaxial tensile, 1D-: cyclic uniaxial compressive, 2D: biaxial, U: cyclic tension-compression (unilateral effect).

Cyclic uniaxial tension and compression tests

Numerical concrete models are compared with the cyclic uniaxial tension and compression loading-unloading experimental test of Gopalaratnam & Shah [41] and Karsan & Jirsa [42], respectively. Figs. 2 and 3 show the response of the three concrete models under tension and compression loads, respectively. It can be observed that all models, except for the DPH model, fit well the post-peak backbone responses of both experimental tests. The UNI model gives the best estimation of the experimental backbones. However, this model fails in predicting the unloading branches since they neglect the plastic strains. In contrast, the unloading branches predicted with the FOC model is closer to the experimental response since this model include plastic strains and stiffness degradation.

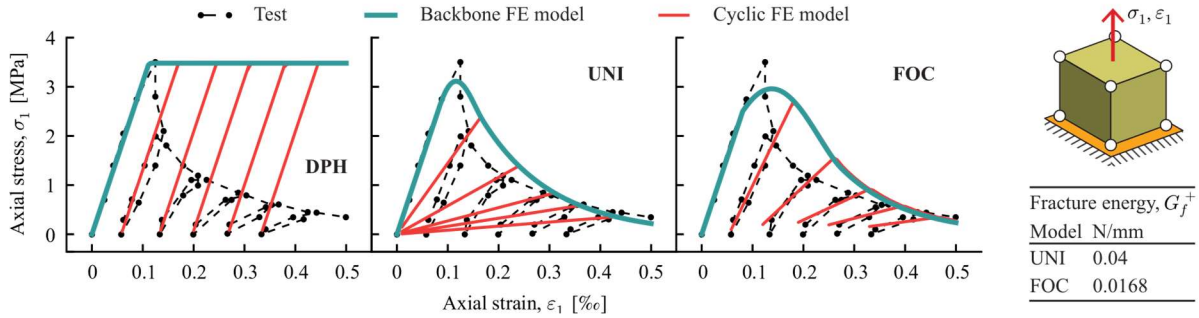

Fig. 2– Validation for the three concrete models under cyclic uniaxial compressive test of Gopalaratnam & Shah [41]. Additional parameters considered: DPH model- f_y^+=3.48MPa, f_y^-=12MPa, $R_1=f_c'/f_y^-$ and R_2=3; and FOC model- B^+=0 and B^-=0.54.

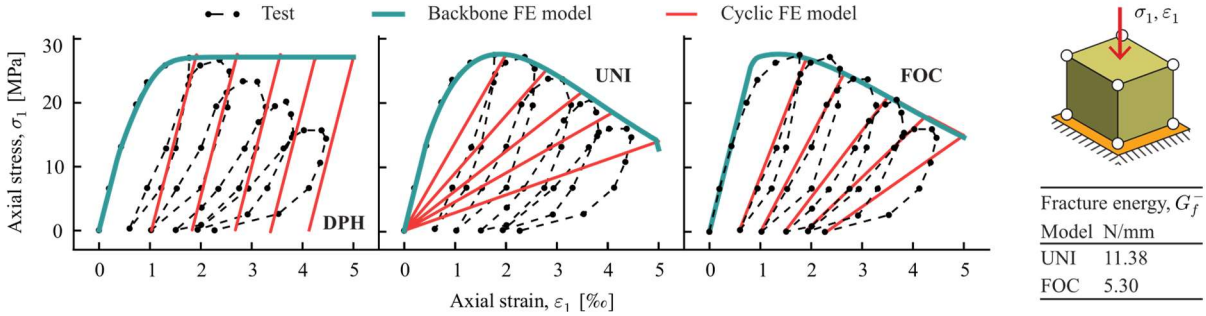

Fig. 3– Validation for the three concrete models under cyclic uniaxial compressive test of Karsan & Jirsa [42]. Additional parameters considered: DPH model- f_y^+=3.48MPa, f_y^-=12MPa, $R_1=f_c'/f_y^-$, R_1=1, and R_2=3; and FOC model- B^+=0 and B^-=0.54.

Monotonic biaxial tests

All concrete models are compared with the monotonic biaxial tests of Kupfer *et al.* [43]. Each test was performed with a constant biaxial loading ratio $a = \sigma_1/\sigma_2$, where σ_1 and σ_2 are the imposed stresses. A pure biaxial stress state is assumed for the boundary conditions to simulate the experimental conditions. A stress-controlled test is performed for all models up to peak stress, except for the uniaxial case (a=0), where a

displacement-controlled test was performed. The input parameters were chosen to fit the cases for α=0, 1, and 0.52 simultaneously.

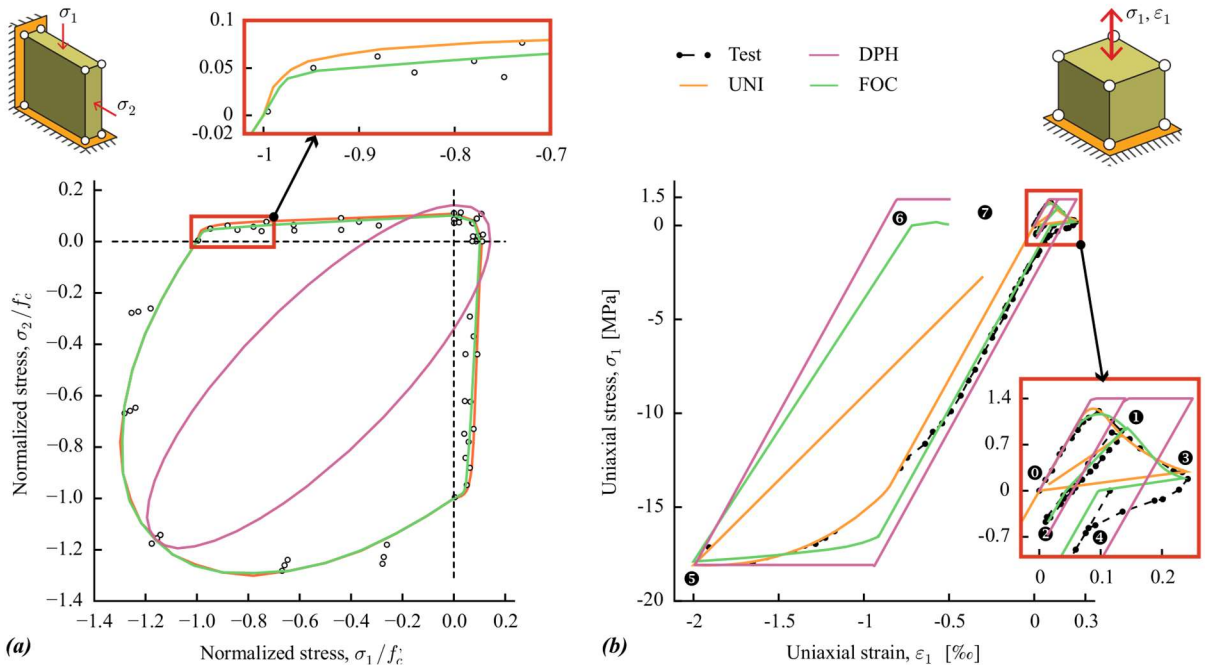

Fig. 4– Validation for the three concrete models under multi-axial stress loadings: (a) biaxial strength envelope for the test result of Kupfer *et al.* [43]; and (b) cyclic tension-compression test of Mazars *et al.* [44]. Additional parameters considered for biaxial test: DPH model- f_y^+=3.5 MPa and $f_y^- = f_b'$; and FOC model- B^+=0.54 and B^-=0.75. For the cyclic tension-compression test: DPH model- R_1=1 and R_2=1; and FOC model- B^+=0.54 and B^-=0.75.

Fig. 4a shows the biaxial strength envelope predicted by the three concrete models. The envelopes were obtained using a different combination of biaxial loading ratios α. For the DPH model, the parameters η and χ were fitted with the tensile/compressive biaxial strength of concrete (see Figs. 1c-d). It is apparent that all models predict closely the experimental envelope in the Compression-Compression (C-C) regime, where the models are mainly influenced by the second-deviatoric stress invariant J_2. Differences among models are also observed in the Tension-Compression (T-C) regimes. The DPH model predicts an adequate response for the C-C regime only for a biaxial loading ratio α=1.

Cyclic tension-compression uniaxial test (unilateral)

To validate the crack closure phenomena (unilateral effect), all concrete models were compared with the cyclic uniaxial test of Mazars *et al.* [44]. The concrete test was first subjected to uniaxial tension followed by uniaxial compression. Fig. 4b shows the experimental and predicted axial stress σ_1 vs axial strain ε_1. The figure shows that the UNI and FOC models recover the initial elastic stiffness once the load goes into the compression state (steps 2 and 4 in Fig. 4b). Moreover, it is observed that only the FOC model follows adequately the experimental compression backbone branch (step 4 to 5), because they include plastic strain in their formulation. Also, it is observed that the FOC model recover the damaged stiffness obtained in the last cycle of tension (step 3) when the load goes from compression to tension state (step 6). This condition is also predicted by the UNI model (not shown in the plot) since this model has the so-called *damage memory*, which is inherent in the thermodynamics irreversible processes. Finally, the DPH model fits well only at the hardening tensile/compressive backbone branch, due that is a plastic model.

4. Uncertainty estimation

To measure the uncertainty on the studied inelastic concrete models, ten response parameters were considered: (**1-2**) peak stress σ_p and respective strain ε_p of the monotonic stress-strain curve; (**3**) dissipated energy of the monotonic E_m stress-strain curve; (**4-6**) dissipated energy of the first E_{c_1}, last E_{c_∞}, and total E_c loading-unloading cycle of stress-strain curve; (**7-8**) linearized least square stiffness of hardening branch $\bar{K}_h$ and softening branch $\bar{K}_s$ of the monotonic stress-strain curve; and (**9-10**) first $\bar{K}_{c_1}$ and last $\bar{K}_{c_\infty}$ linearized least square stiffnesses in loading-unloading cycle. Fig. 5 illustrates these parameters for clarification.

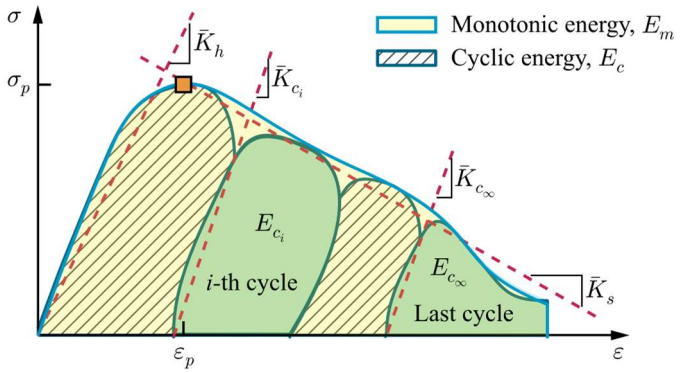

Fig. 5– Definition of response parameters used to measure the epistemic uncertainty for the concrete models.

The uncertainty is measured for the four experimental cases previously analyzed and considering the same input parameters. For all these cases, the ratio of the simulated response R_{num} and the experimental result R_{exp} was calculated. The uncertainty was quantified as the minimum, maximum, and standard deviation (σ) of the ratios $R_{\text{num}}/R_{\text{exp}}$. Fig. 6 summarizes the epistemic uncertainty of the studied models for the uniaxial, biaxial, and unilateral simulations, respectively. The boxplots considered hereafter contains a rectangle whose length is the difference between the first quantile Q_1 and third quartile Q_3, a median Q_2 represented by an intermediate horizontal line, a mean $\bar{x}$ represented by a rhombus, whiskers equivalent in width to two standard deviations (2σ), and outliers, which fall outside the range ($\bar{x} \pm \sigma$) (see remark of Fig. 6a).

First, for the uniaxial tensile regime, the three models predict a good fit for the variables σ_p, ε_p, E_{c_1}, and $\bar{K}_h$, where a standard deviation is less than 15%, whereas for the uniaxial compressive regime the uncertainty for the variables σ_p, ε_p, E_m, and E_c is less than 17%. Conversely, the largest source of error is measured for the energy dissipated by the last cycle E_{c_∞} in the tensile regime, with σ=141.1%; and for the loading-unloading stiffness of the last cycle K_{c_∞} for the tensile and compressive regimes, with σ=338.3% and 223.3%, respectively. The main reason for this high uncertainty is due to the differences in the taxonomy of the concrete models considered (plastic, damage, or plastic-damage). Additional observations can be derived from Fig. 6a. First, results predict up to 47% less dissipated energy by the first loading-unloading cycle E_{c_1}, and up to 40% larger flexibility for the first loading-unloading stiffness $\bar{K}_{c_1}$ relative to the experimental tests. This is mainly due to the UNI model, which unloads to the origin. Second, ratios as large as 2.68 and 2.41 times more dissipated energy are observed for the monotonic E_m and cyclic E_c tensile regime relative to the experimental test. This is mainly influenced by the DPH plastic model, which neglects the stiffness degradation.

For the biaxial case, the boxplot for each variable corresponds to the combination of all stress ratios simulated $a = \sigma_1/\sigma_2$ with a=0, 1, and 0.52. It can observe a moderated level of error for all response variables measured, with errors less than 71%. Similarly, for the uniaxial cyclic tension-compression case (unilateral effect), the standard deviation of all parameters, excepting the variable K_{c_∞}, is less than 33%. In both cases, the unloading-loading stiffness of the last cycle K_{c_∞} is the variable that generates the most source of error, with σ=70.1% and 170.6% for the biaxial and the tension-compression test, respectively.

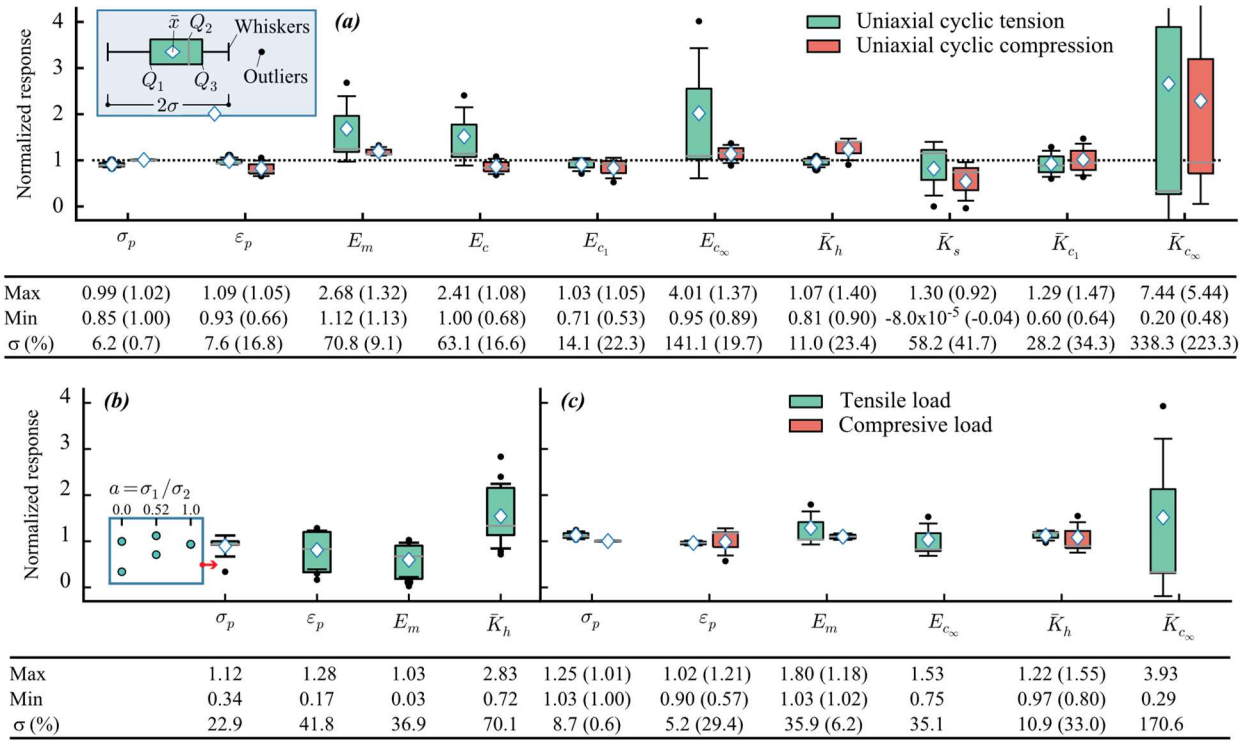

	σ_p	ε_p	E_m	E_c	E_{c_1}	E_{c_∞}	$\bar{K}_h$	$\bar{K}_s$	$\bar{K}_{c_1}$	$\bar{K}_{c_\infty}$
Max	0.99 (1.02)	1.09 (1.05)	2.68 (1.32)	2.41 (1.08)	1.03 (1.05)	4.01 (1.37)	1.07 (1.40)	1.30 (0.92)	1.29 (1.47)	7.44 (5.44)
Min	0.85 (1.00)	0.93 (0.66)	1.12 (1.13)	1.00 (0.68)	0.71 (0.53)	0.95 (0.89)	0.81 (0.90)	$-8.0\text{x}10^{-5}$ (-0.04)	0.60 (0.64)	0.20 (0.48)
σ (%)	6.2 (0.7)	7.6 (16.8)	70.8 (9.1)	63.1 (16.6)	14.1 (22.3)	141.1 (19.7)	11.0 (23.4)	58.2 (41.7)	28.2 (34.3)	338.3 (223.3)

	σ_p	ε_p	E_m	$\bar{K}_h$	σ_p	ε_p	E_m	E_{c_∞}	$\bar{K}_h$	$\bar{K}_{c_\infty}$
Max	1.12	1.28	1.03	2.83	1.25 (1.01)	1.02 (1.21)	1.80 (1.18)	1.53	1.22 (1.55)	3.93
Min	0.34	0.17	0.03	0.72	1.03 (1.00)	0.90 (0.57)	1.03 (1.02)	0.75	0.97 (0.80)	0.29
σ (%)	22.9	41.8	36.9	70.1	8.7 (0.6)	5.2 (29.4)	35.9 (6.2)	35.1	10.9 (33.0)	170.6

Fig. 6– Response parameters of the numerical concrete models normalized by the experimental benchmark test results: (a) uniaxial cyclic tension and compression; (b) biaxial monotonic; and (c) uniaxial cyclic tension-compression. Boxplot diagram (top); and maximum, minimum, and standard deviation σ (%) (bottom). (For cases a and c, values in parenthesis are associated with the compressive load case.)

4. Conclusions

Uncertainty of three three-dimensional stress-strain constitutive concrete models has been studied by comparing model responses in simple benchmark examples. A brief description of these models in a common tensorial notation was presented, providing some recommendations for their numerical implementation and improved convergence. Moreover, numerical benchmark test examples under uniaxial, biaxial, and tension-compression stresses demonstrate the different capacities of the models considered.

The uncertainty observed in the response of a concrete prism is enough to asses correctly the sensitivity of these concrete models. Thus, it is concluded that the unloading-loading linearized stiffness of the last cycle $\bar{K}_{c_\infty}$ for the four tests provide the most important source of error, with a standard deviation of up to σ=338.3%. This is followed by the dissipated energy in the last cycle E_{c_∞} in the uniaxial cyclic tensile test, with σ=141.1%. In contrast, low errors were observed for peak stresses σ_p in all test simulations, and σ <23%.

4. Acknowledgements

This research has been funded by grants Research Center for Integrated Disaster Risk Management (CIGIDEN), CONICYT/ FONDAP/ 15110017; FONDECYT project: SImulation Based Earthquake Risk and Resilience of Interdependent Systems and NetworKs (SIBER-RISK), CONICYT/ FONDECYT/ 1170836; and FONDECYT project: *Concurso Postdoctorado*-2019, CONICYT/ FONDECYT/ 3190680.

5. Copyrights

6. References

[1] PEER Tall building initiative (2017): Guidelines for performance-based seismic design of tall buildings. Report N° 2017/05. Pacific Earthquake Engineering Center.
[2] NIST GCR 17-917-46v1 (2017): Guidelines for nonlinear structural analysis and design of buildings Part I – General. Applied Technology Council.
[3] Chacón MF, de la Llera JC, Hube MA, Marques J, Lemnitzer A (2017): Epistemic uncertainty in the seismic response of RC free-plan buildings. *Engineering Structures*. **141**, 687–702
[4] Jünemann R, de la Llera JC, Hube MA, Vásquez JA, Chacón MF (2016): Study of the damage of Reinforced Concrete shear walls during the 2010 Chile earthquake. *Earthquake Engineering & Structural Dynamics*. **45** (10), 1621–1641.
[5] Almeida J, Tarquini D, Beyer K (2016): Modelling approaches for inelastic behaviour of RC walls: Multi-level assessment and dependability of results. *Archives of Computational Methods in Engineering*. **23** (1), 69–100.
[6] Jünemann R, Vásquez JA, de la Llera JC, Hube MA (2018): Three dimensional inelastic models to assess earthquake damage of reinforced concrete wall buildings. *11th US National Conference on Earthquake Engineering*, Los Angeles, California.
[7] Drucker DC, Prager W (1952): Soil mechanics and plastic analysis for limit design. *Quarterly of Applied Mathematics*. **10** (2), 157–165.
[8] Willam KJ, Warnke ED (1975): Constitutive Model for the Triaxial Behavior of Concrete. *Proceedings International Association for Bridge and Structural Engineering*. **19**, 1–30.
[9] Bigoni D, Piccolroaz A (2004): Yield criteria for quasibrittle and frictional materials. *International Journal of Solids and Structures*. **41** (11), 2855–2878.
[10] Kachanov LM (1958): Time of the rupture process under creep conditions. *Izvestiya Akademii Nauk SSSR Otdelenie Tekniches.* (8), 26–31.
[11] Simo JC, Ju JW (1987): Strain- and stress-based continuum damage models—I. Formulation. *International Journal of Solids and Structures*. **23** (7), 821–840.
[12] Faria R, Oliver J, Cervera M (1998): A strain-based plastic viscous-damage model for massive concrete structures. *International Journal of Solids and Structures*. **35** (14), 1533–1558.
[13] Wu JY, Li J, Faria R (2006): An energy release rate-based plastic-damage model for concrete. *International Journal of Solids and Structures*. **43** (3), 583–612.
[14] Ortiz M (1985): A constitutive theory for the inelastic behavior of concrete. *Mechanics of Materials*. **4** (1), 67–93.
[15] Lubliner J, Oliver J, Oller S, Oñate E (1989): A plastic-damage model for concrete. *International Journal of Solids and Structures*. **25** (3), 299–326.
[16] Lee J, Fenves GL (1998): Plastic-damage model for cyclic loading of concrete structures. *Journal of Engineering Mechanics*. **124** (8), 892–900.
[17] Gupta AK, Akbar H (1984): Cracking in Reinforced Concrete Analysis. *Journal of Structural Engineering*. **110** (8), 1735–1746.
[18] Rots JG (1988): Computational modeling of concrete fracture. *PhD thesis at University of Technology*, Delft, The Netherlands.
[19] Caner FC, Bažant ZP (2013): Microplane Model M7 for Plain Concrete. I: Formulation. *Journal of Engineering Mechanics*. **139** (12), 1714–1723.
[20] Behbahani AD, Barros JAO, Ventura-Gouveia A (2015): Plastic-damage smeared crack model to simulate the behaviour of structures made by cement based materials. *International Journal of Solids and Structures*. **73–74**, 20–40.
[21] Červenka J, Papanikolaou VK (2008): Three dimensional combined fracture-plastic material model for concrete. *International Journal of Plasticity*. **24** (12), 2192–2220.
[22] Simo JC, Hughes TJR (1998): Computational Inelasticity. Springer.
[23] de Souza Neto EA, Peric D, Owen DRJ (2008): Computational Methods for Plasticity: Theory and Applications. John Wiley & Sons, Inc.
[24] Pijaudier-Cabot G, Bažant ZP (1987): Nonlocal Damage Theory. *Journal of Engineering Mechanics*. **113** (10), 1512–1533.

[25] Peerlings RHJ, de Borst R, Brekelmans WAM, de Vree JHP (1996): Gradient Enhanced Damage for Quasi-brittle Materials. *International Journal for Numerical Methods in Engineering*. **39** (19), 3391–3403.
[26] Wang WM, Sluys LJ, de Borst R (1998): Viscoplasticity for instabilities due to strain softening and strain-rate softening. *International Journal for Numerical Methods in Engineering*. **40** (20), 3839–3864.
[27] Alembagheri M, Seyedkazemi, M (2014): Seismic performance sensitivity and uncertainty analysis of gravity dams. *Earthquake Engineering & Structural Dynamics*. **44** (1), 41–58.
[28] Valentini G, Hofstetter B (2013): Review and enhancement of 3D concrete models for large-scale numerical simulations of concrete structures. *International Journal for Numerical and Analytical Methods in Geomechanics*. **37** (3), 221–246.
[29] Pivonka P, Ožbolt J, Lackner R, Mang H (2004): Comparative studies of 3D-constitutive models for concrete: application to mixed-mode fracture. *International Journal for Numerical Methods in Engineering*. **60** (2), 549–570.
[30] Martin O (2010): Comparison of different constitutive models for concrete in ABAQUS/Explicit for missile impact analyses. *European Commission Joint Research Centre Institute for Energy*.
[31] Wang Y, Tang Q, Nie X (2017): Comparative investigation on influences of concrete material constitutive models on structural behavior. *Construction and Building Materials*. **144**, 475–483.
[32] Chacón MF, de la Llera JC, Hube MA, Celentano D (2020): Review of 3D continuum stress-strain concrete models-Part I: Numerical implementation and consistent notation. *Submitted to International Journal of Solids and Structures*.
[33] Chacón MF, de la Llera JC, Hube MA, Celentano D (2020): Review of 3D continuum stress-strain concrete models-Part II: Convergence issues, numerical examples and uncertainty estimation. Submitted to *International Journal of Solids and Structures*.
[34] ANSYS (2018): ANSYS Academic Research, Release 15.0. ANSYS, Inc., Canonsburg, Pennsylvania. www.ansys.com.
[35] ABAQUS (2018): ABAQUS, USER's Manual, version 6.12-1. Dassault Systèmes Simulia Corp. www.3ds.com/products-services/simulia/products/abaqus.
[36] Ladeveze P (1983): Sur une Theorie de l'endommagement Anisotrope. *Laboratoire de Mecanique et Technologie*, Cachan, France.
[37] Mazars J, Pijaudier-Cabot G (1989): Continuum damage theory. Application to concrete. *Journal of Engineering Mechanics.* **115** (2), 345–365.
[38] Duvaut G, Lions JL (1972): Les Inequations en Mecanique et en Physique. Dunod, Paris.
[39] Oliver J, Cervera M, Oller S, Lubliner J (1990): Isotropic damage models and smeared crack analysis of concrete. *Procedings 2nd International Conference Computational Aided Analysis Design Concrete Structures*. 945–957.
[40] Mazars J (1986): A description of micro- and macroscale damage of concrete structures. *Engineering Fracture Mechanics*. **25** (5), 729–737.
[41] Gopalaratnam VS, Shah SP (1985): Softening response of plain concrete in direct tension. *ACI Journal proceedings*. **82** (3), 310–323.
[42] Karsan ID, Jirsa JO (1969): Behavior of concrete under compressive loadings. *Journal of the Structural Division, ASCE*. **95** (12), 2543–2564.
[43] Kupfer H, Hilsdorf HK, Rusch H (1969): Behavior of Concrete under Biaxial Stresses. *ACI Journal Proceedings*. **66** (8), 656–666.
[44] Mazars J, Berthaud Y, Ramtani S (1990): The unilateral behaviour of damaged concrete. *Engineering Fracture Mechanics*. **35** (4), 629–635.

